Journal of Crystal Growth 419 (2015) 133–137

Contents lists available at ScienceDirect

Journal of Crystal Growth

journal homepage: www.elsevier.com/locate/jcrysgro

Static sublimation purification process and characterization of LiZnP semiconductor material

Benjamin W. Montag [a,*], Michael A. Reichenberger [a], Nathan Edwards [a], Philip B. Ugorowski [a], Madhana Sunder [b], Joseph Weeks [c], Douglas S. McGregor [a]

[a] Semiconductor Materials and Radiological Technologies (S.M.A.R.T) Laboratory, Kansas State University, Manhattan, KS 66506, USA
[b] Bruker AXS Inc., 5465 E. Cheryl Parkway, Madison, WI 53711, USA
[c] Department of Agronomy, 2004 Throckmorton Plant Sciences Center, Kansas State University, Manhattan, KS 66502, USA

ARTICLE INFO

Article history:
Received 29 September 2014
Received in revised form
25 February 2015
Accepted 1 March 2015
Communicated by Prof. A. Burger
Available online 9 March 2015

Keywords:
A1. Purification
A1. Radiation
A1. X-ray diffraction
B1. Lithium compounds
B2. Semiconducting ternary compounds

ABSTRACT

Refinement of the class $A^{I}B^{II}C^{V}$ materials continue as a candidate for solid-state neutron detectors. Such a device would have greater efficiency, in a compact form, than present day gas-filled ^{3}He and $^{10}BF_3$ detectors. The $^{6}Li(n,t)^{4}He$ reaction yields a total *Q* value of 4.78 MeV, larger than ^{10}B, and easily identified above background radiations. Hence, devices composed of either natural Li (nominally 7.5% ^{6}Li) or enriched ^{6}Li (usually 95% ^{6}Li) may provide a semiconductor material for compact high efficiency neutron detectors. A sub-branch of the III–V semiconductors, the filled tetrahedral compounds, $A^{I}B^{II}C^{V}$, known as Nowotny–Juza compounds, are known for their desirable cubic crystal structure. Starting material was synthesized by combining equimolar portions of Li, Zn, and P sealed under vacuum (10^{-6} Torr) in quartz ampoules, having boron nitride liners, and subsequently reacted in a compounding furnace (Montag et al., 2015, *J. of Cryst. Growth*). A static vacuum sublimation in quartz was performed to help purify the synthesized material. The chemical composition of the *sublimed material* and *remaining material* was confirmed by Inductively Coupled Plasma Optical Emission Spectroscopy (ICP-OES). Lithium was not detected in the sublimed material, however, approximately stoichiometric concentrations of each constituent element were found in the remaining LiZnP material. X-ray diffraction phase identification scans of the *remains material* and *sublimed material* were compared, and further indicated the impurity materials were sublimed away from the synthesized materials. The resulting material from the sublimation process showed characteristics of a higher purity ternary compound.

1. Introduction

Materials containing ^{6}Li, ^{10}B, ^{113}Cd, ^{157}Gd or ^{199}Hg have been considered for solid-state neutron detectors [2–13]. The $^{10}B(n,\alpha)^{7}Li$ reaction is desirable for the ^{10}B microscopic thermal neutron absorption cross section of 3839 b, but boron-based compounds, such as BP, BN, and BAs have shown limited success, and thus far do not appear promising due to crystal growth and materials preparation problems [10–14]. Thin-film coated diode detectors suffer due to their geometry, where only one reaction product can be absorbed in semiconducting material, thereby producing some signals that can be difficult to distinguish from background and gamma-ray induced events [15]. Additionally, depending on the range of the reaction products in the boron material, film thickness is restricted, and therefore thermal neutron absorption is limited, resulting in a maximum intrinsic detection efficiency of approximately 4.5% [15]. Solid-state detectors containing ^{113}Cd and ^{199}Hg devices also have limited detection efficiency due to the low absorption probability of the prompt gamma-rays that result from the $^{113}Cd(n,\gamma)^{114}Cd$ and $^{199}Hg(n,\gamma)^{200}Hg$ reactions [2–5]. The reaction $^{157}Gd(n,\gamma)^{158}Gd$ is desirable for the large ^{157}Gd thermal neutron capture cross section of 240,000 b. Unfortunately, the reaction results in low energy prompt gamma rays and conversion electrons below 220 keV, mostly near 80 keV, which are difficult to discern from background radiations [15]. Finally, ^{6}Li has not been explored to the same extent as other thermal neutron absorbers, and has an intrinsic thermal neutron absorption cross section of 940 b. The reaction produces a total *Q*-value of 4.78 MeV, seen in the following reaction:

$$^{6}Li + {}^{1}_{0}n \rightarrow {}^{3}H(2.73\ MeV) + \alpha(2.05\ MeV). \quad (1)$$

Nowotny–Juza compounds were originally, and are still today, studied for photonic applications [16–18]. The zincblende crystal structure is arranged where the group II atom is located at $\tau_1 = (0, 0, 0)a$ where *a* is the lattice constant, and the group V atom is located at $\tau_2 = (1/4, 1/4, 1/4)a$. The spacious cubic structure allows for lithium atoms to fill the interstitial site at $\tau_3 = (1/2, 1/2, 1/2)a$

* Corresponding author. Tel.: +1 785 532 6480; fax: +1 785 532 7057.
E-mail address: bmontag@ksu.edu (B.W. Montag).

http://dx.doi.org/10.1016/j.jcrysgro.2015.03.002
0022-0248/

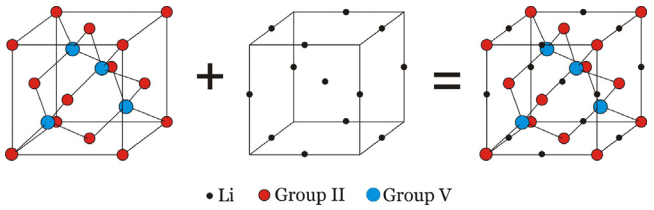

Fig. 1. The Nowotny–Juza filled tetrahedral zincblende cubic crystal structure.

as shown in Fig. 1 [19,20]. The filling of these interstitial sites allows for a lithium-loaded semiconducting material. Further, the concentration of Li atoms in the material is equal to other constituent atoms, as shown in Fig. 1. These material properties make Nowotny–Juza compounds attractive for compact, high neutron sensitivity, solid-state detectors. Difficulties in synthesis, purification, crystal growth, and handling, unfortunately limit the available physical and electrical property data [16–23]. The following study addresses the processes that are necessary for synthesizing phase pure LiZnP material in the powder form. The powders serve as important starting materials necessary for growing high-quality LiZnP crystals, that are necessary for making semiconductor based neutron detectors.

LiZnP material was synthesized in-house, in sealed, crucible-lined quartz ampoules [1,24]. It was noticed that not all synthesis processes yielded high quality material. A multi-step synthesis was performed to yield the highest purity product, although unreacted elemental and binary materials were likely included in the synthesized material [1]. Nowotny–Juza compounds are hygroscopic, thereby, making handling quite difficult. Also, molten lithium reacts with quartz to make lithium silicates, which also narrows available purification techniques [25]. Typical non-solution based purification methods consist of: 1) dynamic vacuum sublimation, 2) static vacuum sublimation, 3) vacuum distillation, and 4) zone refining. Vacuum distillation is typically performed on elemental materials, or compounds, that do not sublime before becoming molten [26,27]. LiZnP melts slightly above 1300 °C, and sublimes before becoming molten, therefore a distillation method is not appropriate. Additionally, due to the high melting temperature, traditional zone refining is not a trivial process. A static vacuum sublimation was chosen over dynamic vacuum sublimation due to little concern of $A^{I}B^{II}B^{V}$ material exposure to the atmosphere in the handling process. Sublimation is a clean and effective way to purify elemental and compounded materials, as shown with many materials [28–30]. Synthesized ternary material was processed through a static vacuum sublimation that significantly helped reduce the material impurity level.

2. Experimental details

The following sections entail the sublimation process of LiZnP, and the ICP-OES and XRD characterization that verify the process results.

2.1. Sublimation process

LiZnP was synthesized, as explained elsewhere [1], in batches up to 2.0 g. Approximately 5.0 g of LiZnP was added to a boron nitride crucible boat, and loaded into one side of a clean, thick-walled (>2.5 mm) quartz ampoule as shown in Fig. 2. The ampoule was removed from the argon atmosphere while remaining under argon by a closed vacuum attachment. The ampoule was placed on a vacuum sealing station, where it was baked out to remove residual moisture, and evacuated to approximately 9.8×10^{-6} Torr, subsequently sealed using a H_2–O_2 torch. The ampoule was placed into a three zone

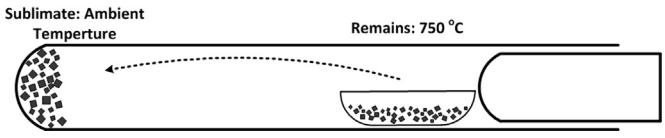

Fig. 2. Diagram of the static sublimation ampoule.

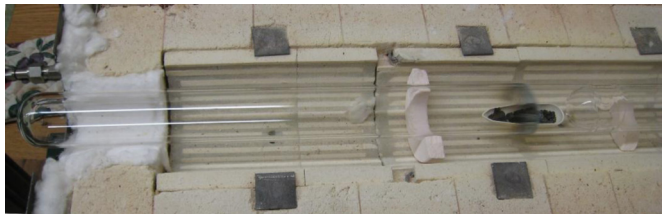

Fig. 3. Ampoule of $A^{I}B^{II}C^{V}$ material prepared for a static sublimation process.

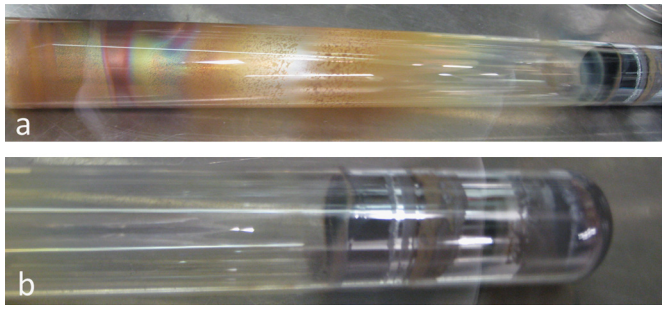

Fig. 4. Ampoule of LiZnP after static sublimation process. (a) The remains end of the ampoule and (b) the sublimed portion of the ampoule.

furnace, where two zones were ramped to 750 °C for LiZnP purification, and the third zone was ramped to 550 °C. The ampoule was also mounted in the furnace so that the cold end of the ampoule extended to the edge of the furnace as shown in Fig. 3.

Samples from each side of the ampoule were collected, one from the *sublimed* material, and one from the remains after purification. Each side of the resulting process ampoule is shown in Fig. 4. The samples were analyzed by elemental analysis on a Varian 720-ES Inductively Coupled Plasma Optical Emission Spectroscopy (ICP-OES) instrument. This method uses simultaneous optical systems, and axial viewing of the plasma to measure characteristic emission spectra by optical spectroscopy. Note, that this particular elemental analysis has been known to have up to a 10% relative standard deviation about the measured elemental weight [31]. However, with careful preparation of the calibration standards, and samples, this relative error can be reduced.

Phase identification x-ray diffraction scans were collected on a Bruker D8 ADVANCE, equipped with Cu radiation, using the Bragg Brentano geometry. A sample from the *sublimed material*, and *remains material* was harvested from the respective side of the purification ampoule, and ground into a fine powder in an argon atmosphere using a clean mortar and pestle. Each powder was loaded into a zero-background sample holder with a layer of Biaxially-oriented polyethyleme terephthalate (BoPET), known as Mylar®, over the top of the material, and sealed for protection from moisture in air. A phase identification scan was collected for both samples. The results were compared with theoretical peak positions calculated with PowderCell 2.4, and data presented in the literature [17,22].

2.2. ICP-OES process

Standard solutions of varying concentrations (0, 1, 3, and 5 mg/L—Li; 0, 15, 30, 50, and 70 mg/L—Zn; 0, 10, 20, 30, and

40 mg/L—P) in water were prepared, and measured on a Varian 720-ES ICP-OES instrument to establish concentration curves. Percent deviation, or error, from the expected concentration of each standard solution was determined by the instrument, the results of which, can be found in Table 1. The LiZnP *remains material* and *sublimed material* were prepared for ICP-OES analysis. Each 100 mg sample was loaded into a pyrex sample container under argon, and sealed with Parafilm© to reduce air exposure when removed from the glove box. In a fume hood, the Parafilm© was removed, and 10 mL of freshly prepared aqua regia (1:4 volumetric ratio HNO_3/HCl) was quickly added to each sample. The remains side of LiZnP purification produced a noticeable reaction that produced a black vapor with the addition of aqua regia. The addition of aqua regia to the deposition side did not produce a noticeable reaction. The digestion was allowed to continue overnight.

Most of the material had dissolved in each sample vial after a 24 h period. To ensure complete digestion of the remaining material, each vial was heated on a digestion block at 75 °C for 30 min, 100 °C for 30 min, 110 °C for 30 min, and 140 °C until the acid was reduced to approximately 2.0 mL [32]. Each solution was removed from the digestion block and was increased to a 50 mL solution using 0.1% HNO_3. Each 50 mL solution was then filtered through a Whatman© no. 42 filter paper. A 2.5 mL sample from each filtrate was diluted a second time to 50 mL, to acquire a solution possessing less than 100 mg/L of each element of interest. Some sample solutions still exceeded detection limits of the ICP-OES instrument, so further dilution by 25% or 50% was required. Two measurements were collected for each sample.

The analysis results are listed in Table 2. The percent result of each constituent element was based on the instrument analysis of the concentration of the particular element, and the total amount of material originally weighted for analysis. The elemental percent concentrations were then converted to molar concentration using each element's molar mass. The analysis percent error, and molar concentration standard error were determined based on the deviation from the average of the two measurements for each sample, and the systematic error associated with the concentration curves determined by the ICP-OES instrument.

3. Results and discussion

Static vacuum sublimation of the in-house synthesized powders and chunks of LiZnP appeared to produce a higher purity ternary material. Listed in Table 2 are the ICP-OES results for a LiZnP purification collected on a Varian 720-ES Inductively Coupled Plasma Optical Emission Spectrometer. Li was only slightly present in the *sublimed material* sample with a concentration of $< 0.1\%$. The *remains material* kept the stoichiometric ratios desired for $A^{I}B^{II}C^{V}$ materials with a Li concentration of $13.05 \pm 0.09\%$. Furthermore, the total weight percent of each *remains material* element equaled 100% within the propagated total 3.3% error from the three elemental measurements. Additionally, each elemental constituent molar concentration is approximately equal within the standard deviation. These results further indicate that impurities (binaries, unreacted elemental components) were transferred out of the in-house synthesized material during the sublimation process, leaving a much purer ternary material.

The theoretical peak positions for LiZnP with a lattice constant of 5.751 ± 0.001 Å, as calculated using PowderCell 2.4 is shown in Fig. 5 [33]. The x-ray diffraction phase identification results of the *sublimed material* and *remains material* are shown in Figs. 6 and 7 respectively. The *sublimed material* did not indicate many Bragg reflections, therefore making it difficult to identify. However, the *remains material* phase identification, shown in Fig. 7, showed an arrangement of peaks that match with what is presented in the literature [17,22] and from what was theoretically calculated (Fig. 5). A lattice constant was determined using TOPAS (Bruker AXS Inc.). The Whole Pattern decomposition approach was used. Refinement of the *remains material*

Table 1
The standard solution percent errors, or deviations, from the expected concentrations. Negative values indicates the concentration deviation lies below the expected value.

Element	Concentration (mg/L)	% Error
Li	0	0
	1	5.116
	3	0.554
	5	−0.404
Zn	0	0
	15	7.151
	30	8.493
	50	3.184
	70	−3.513
P	0	0
	10	0.356
	20	0.813
	30	−0.404
	40	0.002

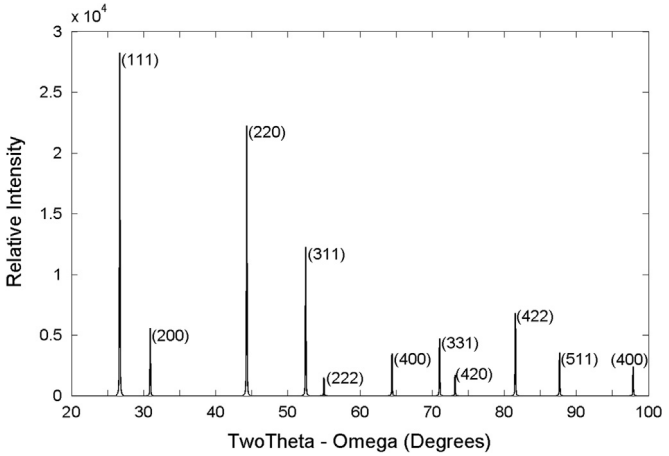

Fig. 5. The theoretical Cu x-ray phase identification of LiZnP. Calculated using PowderCell 2.4 [33]. A 5.751 ± 0.001 Å lattice constant and F-43 m space group was used in the calculation as reported elsewhere [1].

Table 2
The ICP-OES results of LiZnP post static sublimation collected on a Varian 720-ES.

Sample: remains (purified)			Sample: sublimate (elemental, binary)		
Analysis	Result (weight %)	Molar concentration (mol/L)	Analysis	Result (weight %)	Molar concentration (mol/L)
P	33.0 ± 0.4	0.001011 ± 0.000004	P	23.0 ± 0.3	0.000780 ± 0.000003
Li	13.05 ± 0.09	0.001786 ± 0.000002	Li	< 0.1	
Zn	54.3 ± 2.8	0.00079 ± 0.00002	Zn	85.6 ± 2.3	0.001375 ± 0.000004
Total	100.4 ± 3.3				

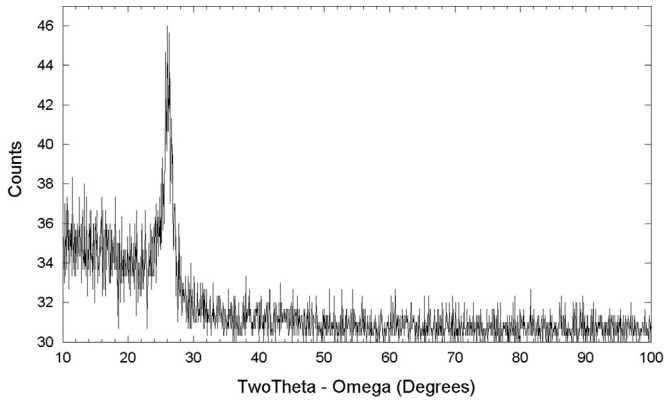

Fig. 6. LiZnP *sublimed material* phase identification scan collected on a Bruker AXS D8 ADVANCE equipped with Cu radiation, using the Bragg Brentano geometry.

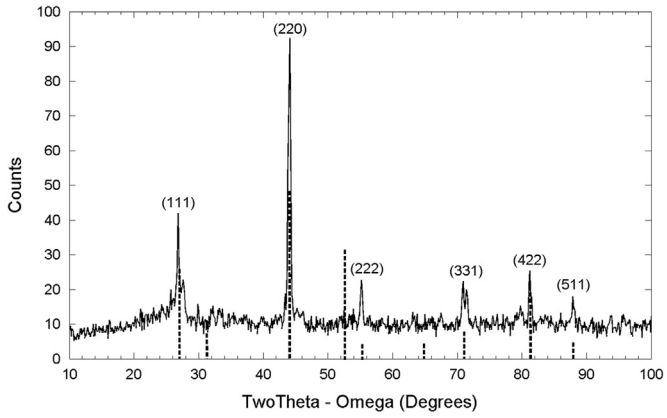

Fig. 7. LiZnP *remains material* phase identification scan collected on a Bruker AXS D8 ADVANCE equipped with Cu radiation, using the Bragg Brentano geometry. The black vertical dotted lines are experimental peaks found by Bacewicz [22].

phase identification data yielded a lattice constant of 5.786 ± 0.002 Å which was consistent to what was reported from raw synthesized (unpurified) material [1].

The *remains material* phase identification, Fig. 7, clearly showed the (111), (220), (222) (331) (422) and (511) LiZnP orientations. In addition preferred orientation along the (220) LiZnP is observed. However, the (200), (311), (400) and (420) orientations are not recorded. The (200), (400) and (420) LiZnP orientations do have weak reflections, as seen in Fig. 5, and therefore, can be difficult to measure. Additional peaks were also observed near the (111) and (331) LiZnP orientations which could be due to secondary phases created as a result of oxidation during handling and measurement. The material was encapsulated under argon during the measurement, and degradation could have occurred over time due to leakage of air into the encapsulant. Additionally there is also the possibility of the presence of a secondary LiZnP phase with a slightly different lattice constant. Ultimately, the static sublimation process appeared to help clean the LiZnP material of unreacted metals, or other impurities, as clearly shown by comparison between Figs. 6 and 7.

4. Conclusions

Nowotny–Juza compounds were synthesized in-house into powder and chunks, and purified by a static sublimation. The ICP-OES data indicate that higher vapor pressure binary and elemental materials can be removed from the synthesized material reducing the impurity level, while retaining the 1:1:1 stoichiometric ratio between constituent elements. The purification material X-ray diffraction studies also indicate that impurities were removed. However, some secondary phases remain, and could belong to a binary or elemental material that was included from one or a few of the five total LiZnP synthesis processes that were used in the sublimation process. Additionally, the thermal profile may have to be explored further to optimize the sublimation process. Ultimately, a higher quality material was produced, and will be used to grow crystalline ingots that can be processed into devices. Finally, electrical properties (resistivity, electron mobility) and neutron sensitivity will be characterized from these devices.

Acknowledgments

The authors express gratitude to John Desper, and the Kansas State University Chemistry department for the use of their Bruker D8 ADVANCE X-ray diffractometer. Work funded in part by the Advanced Materials program DOE—NNSA, Grant DE-FEG52-08NA28766.

References

[1] B.W. Montag, M.A. Reichenberger, K.R. Arpin, et al., Synthesis and characterization of LiZnP and LiZnAs semiconductor material, J. Cryst. Growth 412 (2015) 103–108.
[2] Z.W. Bell, K.R. Pohl, L. Van Den Berg, Neutron detection with mercuric iodide, IEEE Trans. Nucl. Sci. 51 (3) (2004) 1163–1165.
[3] A.G. Vradii, M.I. Krapivin, L.V. Maslova, et al., Possibilities of recording thermal neutrons with cadmium telluride detectors, Sov. At. Energy 42 (1) (1977) 64–66.
[4] A.G. Beyerle, K.L. Hull, Neutron detection with mercuric iodide detectors, Nucl. Instum. Methods A 256 (2) (1987) 377–380.
[5] D.S. McGregor, J.T. Lindsay, R.W. Olsen, Thermal neutron detection with cadmium$_{1-x}$ zinc$_x$ telluride semiconductor detectors, Nucl. Instum. Methods A 381 (2) (1996) 498–501.
[6] Y. Kumashiro, K. Kudo, K. Matsumoto, et al., Thermal neutron irradiation experiments on ^{10}BP single-crystal wafers, J. Less Common Met. 143 (1–2) (1988) 71–75.
[7] W.C. McGinnis, Film implementation of a neutron detector (find): proof of concept device, Technical report 1921, 2003.
[8] J.C. Lund, F. Olschner, F. Ahmed, et al., Boron phosphide on silicon for radiation detectors, MRS Online Proc. Libr. 162 (1989) 601–604.
[9] F.P. Doty, Boron nitride solid state neutron detector, US-6727504, April 27, 2004.
[10] A.N. Caruso, P.A. Dowben, S. Balkir, et al., The all boron carbide diode neutron detector: comparison with theory, Mater. Sci. Eng. B 135 (2) (2006) 129–133.
[11] B.W. Robertson, S. Adenwalla, A. Harken, et al., A class of boron-rich solid-state neutron detectors, Appl. Phys. Lett. 80 (19) (2002) 3644–3646.
[12] P. Groot, J.H.F. Grondel, P.J.v.d. Put, Chemical vapour deposition of boron phosphides using bromide etchants, Solid State Ion. 16 (1985) 95–98.
[13] A.N. Caruso, R.B. Billa, S. Balaz, et al., The heteroisomeric diode, J. Phys. Condens. Matter 16 (2004) L139–L146.
[14] D.S. McGregor, T.C. Unruh, W.J. McNeil, Thermal neutron detection with pyrolytic boron nitride, Nucl. Instum. Methods A 591 (3) (2008) 530–533.
[15] D.S. McGregor, M.D. Hammig, Y.H. Yang, et al., Design considerations for thin film coated semiconductor thermal neutron detectors—I: basics regarding alpha particle emitting neutron reactive films, Nucl. Instum. Methods A 500 (1–3) (2003) 272–308.
[16] R. Juza, K. Langer, K. Von Benda, Ternary nitrides, phosphides, and arsenides of lithium, Angew. Chem. Int. Ed. Engl. 7 (5) (1968) 360–370.
[17] H. Nowotny, K. Bachmayer, Die Verbindungen LiMgP, LiZnP und LiZnAs, Monatshefte Chem. Verwandte Teile And. Wissenschaften 81 (4) (1950) 488–496.
[18] D. Kieven, A. Grimm, A. Beleanu, et al., Preparation and properties of radio-frequency-sputtered half-Heusler films for use in solar cells, Thin Solid Films 519 (6) (2011) 1866–1871.
[19] K. Kuriyama, T. Katoh, N. Mineo, Crystal growth and characterization of the filled tetrahedral semiconductor lithium zinc phosphide (LiZnP), J. Cryst. Growth 108 (1–2) (1991) 37–40.
[20] K. Kuriyama, T. Katoh, Optical band gap of the filled tetrahedral semiconductor lithium zinc phosphide (LiZnP), Phys. Rev. B: Condens. Matter 37 (12) (1988) 7140–7142.
[21] K. Kuriyama, T. Katoh, S. Tsuji, Preparation and characterization of the filled tetrahedral semiconductor lithium zinc phosphide film on quartz, J. Appl. Phys. 66 (8) (1989) 3945–3947.
[22] R. Bacewicz, T.F. Ciszek, Preparation and characterization of some $A^{I}B^{II}C^{V}$ type semiconductors, Appl. Phys. Lett. 52 (14) (1988) 1150–1151.

[23] R. Bacewicz, T.F. Ciszek, Crystal growth and characterization of some novel $A^{I}B^{II}C^{V}$ semiconductors, Acta Phys. Pol. A A77 (2–3) (1990) 379–381.
[24] B.W. Montag, K.A. Nelson, M.A. Reichenberger, et al., Growth and preparation of LiZnP and LiZnAs for solid-state neutron detectors, in: Proceedings of the 2011 IEEE Nuclear Science Symposium (NSS/MIC), 23–29 October, 2011, pp. 1742–1744.
[25] L.F. Epstein, W.H. Howland, The distillation of lithium metal, Science 114 (2965) (1951) 443–444.
[26] S.T. Ali, D.S. Prasad, N.R. Munirathnam, et al., Purification of tellurium by single-run multiple vacuum distillation technique, Sep. Purif. Technol. 43 (3) (2005) 263–267.
[27] A.M. Hageman, M.J. Harrison, N. Fritz, et al., Purification of tellurium to 6 N using a multistage vacuum distillation method, Proc. SPIE 6707 (2007) 67070Z–67077Z.
[28] G.W. Frances, Chemical Experiments; The Theory, Practice, and Application of the Science of Chemistry, and Containing the Properties, Uses, Manufacture, Purification, and Analysis of all Inorganic Substance: With Numerous Engravings of Apparatus, etc., G. Berger, England, 1842.
[29] M. Schieber, R.C. Carlston, H.A. Lamonds, et al., Purification, growth, and characterization of alpha mercuric-iodide crystals for gamma-ray detection, J. Cryst. Growth 24–25 (1974) 205–211.
[30] V.M. Zaletin, N.V. Lyakh, I.N. Nozhkina, Mass transport during growing mercuric iodide by static sublimation method, Cryst. Res. Technol. 20 (3) (1985) 321–327.
[31] Galbraith Laboratories Inc., GLI method summary: inductively coupled plasma atomic emission spectrometry.
[32] H.L. Premarathna, M.J. McLaughlin, J.K. Kirby, et al., Potential availability of fertilizer selenium in field capacity and submerged soils, Soil Sci. Soc. Am. J. 74 (5) (2010) 1589–1596.
[33] W. Kraus, G. Nolze, Powder cell—a program for the representation and manipulation of crystal structures and calculation of the resulting X-ray powder patterns, J. Appl. Crystallogr. 29 (3) (1996) 301–303.